Vietnam Journal of Science and Technology ***63*** *(1) (2025) 111-122*

doi:10.15625/2525-2518/19250

Floating photocatalyst based on Fe doped TiO_2 immobilized on vermiculite for degradation of ciprofloxacine

Nguyen Thi Hue[1, 2, *], Chu Viet Hai[1], Vu Van Tu[1], Nguyen Xuan Dat[1], Luu Van Huyen[3], Nguyen Manh Nghia[4]

[1]*Institute of Environmental Technology, Vietnam Academy of Science and Technology (VAST), A30 building, 18 Hoang Quoc Viet Street, Cau Giay District, Ha Noi, Viet Nam*

[2]*Graduate University of Science and Technology, VAST, A28 building, 18 Hoang Quoc Viet Street, Cau Giay District, Ha Noi, Viet Nam*

[3]*Hanoi University of Natural Resources and Environment, 41 A Phu Dien Road, Bac Tu Liem District, Ha Noi, Viet Nam*

[4]*Faculty of Physics, Hanoi National University of Education, 136 Xuan Thuy Street, Cau Giay District, Ha Noi, Viet Nam*

[*]Email: *nthue2003@gmail.com*

Received: 23 October 2023; Accepted for publication: 31 December 2024

Abstract. In this work, a floating photocatalyst based on Fe-doped TiO_2 immobilized on vermiculite is synthesized via sol gel process. Samples were characterized by X-ray diffraction, N_2 isothermal loops, scanning electron microscopy, high-resolution transmission electron microscopy, and ultraviolet - visible absorption to find its crystal phase composition, particle size, porosity, morphology, and light absorption ability, respectively. The specific surface area of natural vermiculite increased from 6 to 323 m^2/g by pretreatment with 40 % HNO_3 solution. TiO_2 crystalline anatase was combined with a vermiculite support to form a floating photocatalyst. The enhanced visible light absorption was achieved by adding 0.6 % mol Fe dopant to the TiO_2 structure. The total adsorption and photocatalytic efficiency in the ciprofloxacine degradation of Fe-doped TiO_2 immobilized vermiculite was approximately 60 % while that of pure TiO_2 immobilized vermiculite was only about 40 %. This result showed the improvement of floating photocatalysts in degrading antibiotics in water using visible light.

Keywords: Ciprofloxacin, Fe doped TiO_2, floating photocatalyst, vermiculite.

Classification numbers: 2.4.2, 3.4.2, 3.6.1.

1. INTRODUCTION

Today, ciprofloxacin is one of the most commonly prescribed antibiotics detected in hospital wastewater, domestic sewage and surface water with a concentration ranging from ng/L to μg/L [1 - 4]. The wide-spectrum use of ciprofloxacin and inadequate water treatment systems

are the main causes of water pollution by this antibiotic [5, 6]. Ciprofloxacin residues in water environments lead to a number of toxic effects such as promoting bacterial resistance, warning algae growth, and disrupting the N cycle involved in microorganism [1]. Unfortunately, traditional water treatment techniques such as filtration, adsorption, flocculation, chemical precipitation, and biological processes can be ineffective, expensive, energy-consuming and can also lead to the formation of by-products [7]. Therefore, heterogeneous photocatalysis, a potential method to remove persistent pollutants has been investigated by many researchers, in which TiO_2 is one of the most commonly used photocatalytic materials [4].

Research results have shown that TiO_2 photocatalyst has good potential to treat ciprofloxacin in real water samples. At laboratory scale, the optimum conditions including light source, solution pH, irradiation time and catalyst dose for the degradation of ciprofloxacin at high concentrations into the smallest product using TiO_2 nanoparticles were found [8]. Several structural modifications of TiO_2 were made by Zn [9], N [10], S [11] dopants to expand its natural light absorption. The heterojunction between TiO_2 and other semiconducting oxides such as SnO_2 [12], Fe_2O_3 [13], g-C_3N_4 [14] was created for improving the efficiency of decomposing organic pollutants. The immobilization of TiO_2 on a support like glass plate [15] and ceramic [16] was developed to solve the problem of catalyst reuse.

On the other hand, the immobilization of TiO_2 with floating supports is expected to bring the catalyst technology to treat wastewater in a real water environment and the non-stirred reactions is the notable advantage of this photocatalyst material [17]. Preliminary results show that vermiculite, a non-toxic natural clay mineral, can be used as a substrate to form floating photocatalysts. The vermiculite formed from tetrahedral SiO_4 layers and octahedral $Al(OH)_3$ or $Mg(OH)_2$ layers is mechanically and thermally resistant [18]. A fascinating property is that its low density (0.05-0.30 g/cm^3) leads to vermiculite's ability to float on water, so the TiO_2 nanoparticles dispersed on vermiculite can be recovered and recycled after the treatment is complete. Furthermore, the TiO_2 immobilized vermiculite with increased surface area of TiO_2 demonstrated an enhancement of the photocatalytic adsorption performance of the photocatalytic material [12].

In this study, natural vermiculite was treated with HNO_3 to have porous support and TiO_2 photocatalyst was doped by Fe to form a floating material that has both adsorption and photocatalyst functions in ciprofloxacin treatment. Changes in the structure, surface morphology, absorption spectra and porosity of the vermiculite-TiO_2 composite were investigated. Moreover, based on fluidized-bed reactor, the ciprofloxacin degradation by synthesized samples under visible illumination is also examined to find its potential applications in the real wastewater photocatalytic treatment.

2. MATERIALS AND METHODS

2.1. Chemicals

Titanium (IV) isopropoxide (TTIP, $C_{12}H_{28}O_4Ti$, 98 %, Deajung, Korean), ($Fe(NO_3)_3.9H_2O$, 99 %, China), diethanolamine (DEA, Sigma-Aldrich Co. LLC), and ethanol (EtOH, C_2H_5OH, 98 %, Deajung, Korea) were used for preparing sol solutions. Deionized water was used throughout the experiment. The natural vermiculite (ver) clay used in this work was achieved from Son Binh sericite (Ha Tinh province, Viet Nam) with the properties listed in Table 1. Nitric acid (HNO_3, 65 %, Merck, Germany) was used in vermiculite treatment process.

Table 1. Characteristics of natural vermiculite.

Parameter	Component				Dry density	Cation-Exchange capacity (CEC)	pH
	SiO_2	Al_2O_3	Fe_2O_3	MgO			
Value	47.2 %	8.5 %	5.4 %	9.8 %	152 kg/m^3	149 meq/100 g	6.8

2.2. Vermiculite modifying

The process of acid modification for vermiculite was as follows: natural vermiculite was washed with deionized water, dried, crushed and sieved though an 80 mesh wire sieve; the vermiculite is then treated with 40 % nitric acid solution at room temperature for 7 days; after being shaken, filtrated and washed with deionized water until pH reached 7, the vermiculite was dried at 105 ^oC for 2 h and then calcined at 600 ^oC for 4 h to obtain samples of vermiculite denatured by HNO_3 (ver/HNO_3).

2.3. Photocatalyst synthesis

Samples were prepared via the sol gel method. The mixture consisting of TTIP, DEA, and EtOH had a molar ratio of 1:1:34, respectively, and was slowly stirred at room temperature for 3 h. The Fe^{3+}-doped TiO_2 sol was obtained by adding $Fe(NO_3)_3.9H_2O$ to the sol solution with a molar ratio of Fe^{3+}/Ti^{4+} = 6 %. Denatured Ver was soaked in the sol solution for 60 min, dried at room temperature for one day and annealed at 500 ^oC for 3 h. The soaking, drying and annealing steps were repeated 3 times for samples of pure and Fe-doped TiO_2 immobilized on vermiculite (TiO_2/ver, Fe-TiO_2/ver).

2.4. Characterization

The crystalline phase of the synthesized samples was determined using an X-ray diffractometer (D8-ADVANCE) in the 2θ angle range of 20^o - 70^o using Cu Kα radiation l = 1.54060 Å. The porosity properties were determined via nitrogen adsorption/desorption isotherms at 77 K using a 3Flex surface characterization analyzer (Micromeritics, USA). The samples were degassed for 180 min in an N_2 environment at 300 ^oC prior to measurement. The specific surface area was calculated by multipoint Brunauer - Emmett - Teller (BET) method. The static volume and the average pore width were calculated using Barrett - Joyner - Halenda (BJH) desorption method. Surface morphology and microstructure were measured by scanning electron microscopy (SEM, S-4800, Hitachi, Japan) and high-resolution transmission electron microscopy (HRTEM, JEM-2100, JEOL). The distribution of elements was analyzed through energy dispersive X-ray spectroscopy (EDS, Tecnai Osiris 200 kV, FEI, USA). The band gap was obtained from the ultraviolet-visible (UV - vis) absorption spectra measured by a V670 system (Jasco, USA).

2.5. Photocatalytic activity test

The photocatalytic performance of the samples was estimated through the degradation reactions of ciprofloxacine under visible irradiation. The photocatalytic set up based on a fixed bed reactor is schematically summarized in Figure 1. Two grams of the sample were loaded into a quartz tube with a diameter of 1 cm and a length of 20 cm. This tube was illuminated by a LED lamp (T8, 60 cm, 10 W, Rang Dong Com., Viet Nam) as a visible light source. Two liters of a

solution containing ciprofloxacine at an initial concentration of 20 ppm were held in a reservoir and circulated through the photocatalytic system using a diaphragm water pump. The flow rate was set at 1 mL/min. A 4 mL sample solution was collected every 60 min for analysis. The concentration of ciprofloxacine in the reservoir was determined using a HPLC, Shimadzu LC-10AD vp with C18 Resteck 4.6 × 150 column, UV-vis SPD 10A Detector at a wavelength of 278 nm; the retention time was 8.25 min.

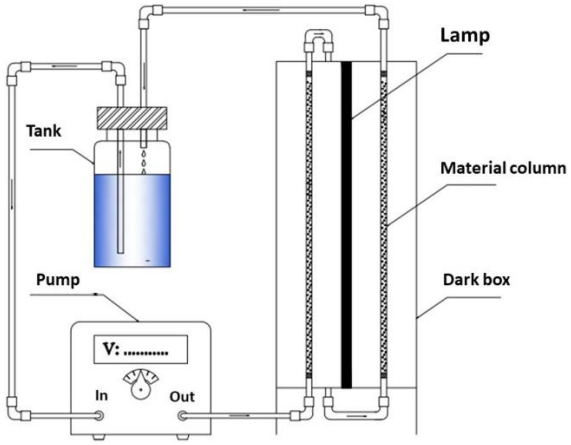

Figure 1. Schematic diagram of photocatalytic set up based on a fixed bed reactor for ciprofloxacine solution degradation.

3. RESULTS AND DISCUSSION

3.1. Crystal phase

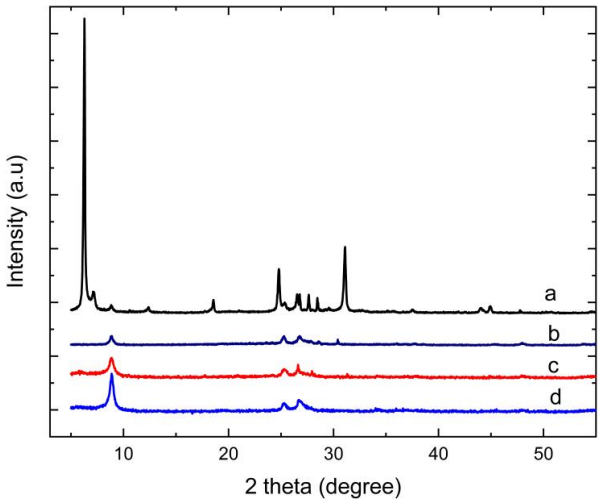

Figure 2. X-ray diffraction of ver (a), ver/HNO_3 (b), TiO_2 /ver (c), and Fe-TiO_2/ver (d) samples.

XRD was analyzed to recognize the crystal structure of the synthesized samples. Figure 2 shows the diffractogram of the TiO_2/ver sample, in which the range of 2θ was chosen from 5^o to 55^o to focus on both vermiculite and TiO_2 phases. The highest peak is at $2\theta = 6.28^o$ related to

the vermiculite (0,0,2) phase of the $Al_{0.721}Fe_{0.24}H_3Mg_{1.338}O_9Si_{1.36}$ composition [17]. This peak disappears in the diffractogram of the vermiculite sample treated by HNO_3. It clearly proves that the delamination was accompanied by the removal of most Mg^{2+} and Al^{3+} ions from the crystal structure and greatly increased the silica content [17]. On the diffraction lines of TiO_2/ver and Fe-TiO_2/ver samples, there were signature diffraction peaks located at 25.3° belonging to (101) lattice plane of anatase phase of TiO_2. These results are in good agreement with our previous studies [19, 20].

3.2. Porosity property

The porosity of a material is one of the most importance factors affecting its adsorption and photocatalytic performance in the treatment of organic pollutants. The nitrogen adsorption-desorption isotherms exhibited in Figure 3 were used to calculate the surface area, pore volume and pore size of our samples. The calculation results given in Table 2 show that the porous characteristics are strongly improved: the specific surface area increases from 6 to 323 m^2/g, the pore volume increases from 0.013 to 0.258 cm^3/g, and the average pore diameter decreases from 123 to 31 Å after HNO_3 treatment process. The adsorption-desorption isotherms of ver/HNO_3 belong to the type IV according to the IUPAC classification. It is possible that porous frames are created when strong nitric acid removed aluminum or silica compounds [17, 18, 21]. Thus, these mesopores are the reason why the amount of N_2 adsorbed onto the sample increases sharply at high pressure due to the capillary effect. It can be seen that vermicurlite treated with nitric acid becomes a good catalyst carrier because of its large specific surface area.

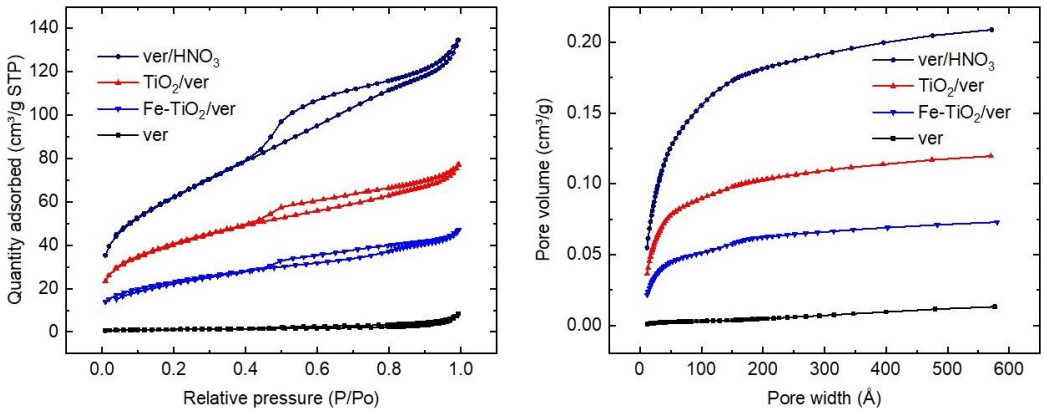

Figure 3. Nitrogen adsorption-desorption isotherms (left) and Horvath-Kawazoe cumulative pore volume plot (right) of samples.

Table 2. Summary of porosity of ver, ver/HNO_3, TiO_2/ver, and Fe-TiO_2/ver samples.

Sample	ver	ver/HNO_3	TiO_2/ver	Fe-TiO_2/ver
BET Surface Area, m^2/g	4	323	140	80
Pore volume, cm^3/g	0.0125	0.2575	0.1190	0.0723
Average pore diameter, Å	123	31	34	36

Adsorption-desorption isotherms of TiO_2/ver and Fe-TiO_2/ver remain the shape of type IV mesoporous materials. Compared with ver/HNO_3 support, the catalyst immobilized samples created a reduction in surface area, from 323 m^2/g to 140 m^2/g, to 80 m^2/g, and the pore volume declined from 0.258 cm^3/g to 0.119 cm^3/g, to 0.072 cm^3/g, respectively. On the other hand, the average pore diameters of acid-treated vermiculite, TiO_2/ver and Fe-TiO_2/ver, were almost the same, which were 31Å, 34Å, 36Å. Furthermore, Horvath-Kawazoe cumulative pore volume plots of TiO_2/ver and Fe-TiO_2/ver were similar to that of ver/HNO_3 sample. These results indicate that TiO_2 or Fe-TiO_2 particles displaced some of the internal pores of the vermiculite carrier material.

3.3. Morphology

The texture and morphology of materials are important in determining their photocatalytic behaviors and activities. Figure 4 shows the SEM images of our samples. The treated vermiculite had a sandwiched structure. The lamellae were stacked together similar to a pack of playing cards. The surface area of the crystalline sandwich was very large compared to the thickness. Evidently, there were few macropores on the vermiculite surface. These findings coincide with the results of the pore size distribution analyses using the BJH method [22]. Numerous micropores and mesopores with diameters less than 50 nm were distributed on the support surface. The flat surface of vermiculite changed to layer stack. These results agree with the XRD and porous results. And, after being treated with acids, vermiculite becomes a good support material. When the catalyst is applied to vermiculite, small round particles appear on the surface of the material with grain sizes in the range of 5 - 10 nm, homogeneously distributed on vermiculite.

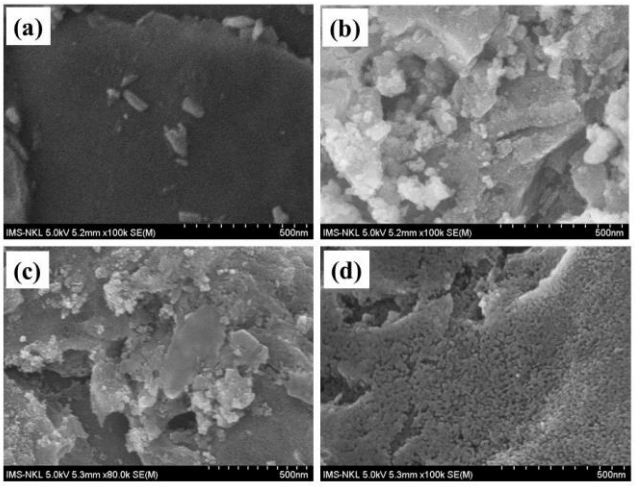

Figure 4. SEM images of ver (a), ver/HNO_3 (b), TiO_2/ver (c), and Fe- TiO_2/ver (d) samples.

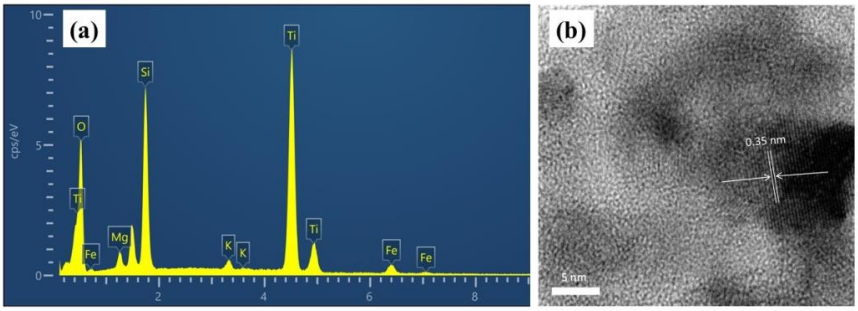

Figure 5. EDS spectra (a) and HR-TEM images (b) of Fe-TiO_2/ver sample.

The chemical composition of the Fe-TiO_2/ver sample was determined through energy dispersive X-ray spectroscopy analysis as shown in Figure 5 and Table 3. This result shows the existence of TiO_2 in the material. The HR-TEM images show that TiO_2 exists in the anatase phase because the perpendicular lattice spaces d_{101} were determined to be 0.35 nm as presented in Figure 5b. From the EDS, SEM, HR-TEM, XRD results, we can confirm that TiO_2 in anatase and vermiculite in $Al_{0.721}Fe_{0.24}H_3Mg_{1.338}O_9Si_{1.36}$ phases exists in the Fe-TiO_2/ver sample.

Table 3. Chemical composition of Fe-TiO_2/ver sample analyzed by EDS technique (removed Al).

Element	Weight %	Weight % Sigma	Atomic %
O	44.77	0.37	66.47
Mg	4.15	0.08	4.05
Si	12.81	0.12	10.83
K	2.17	0.06	1.32
Ti	27.37	0.23	13.57
Fe	8.46	0.18	3.60
Ca	0.27	0.05	0.16
Total	100.00		100.00

3.4. Light absorption

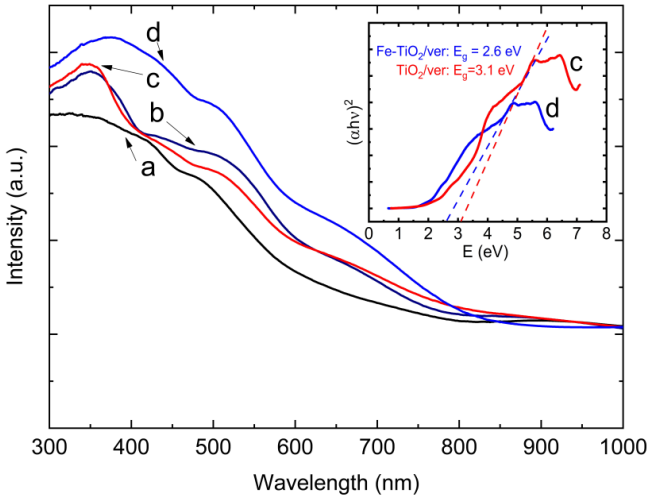

Figure 6. UV-vis spectra of ver (a), ver/HNO_3 (b), TiO_2/ver (c), and Fe-TiO_2/ver (d) samples.

The light harvesting ability of synthesized samples were evaluated by UV-vis DRS spectra as shown in Figure 6. The natural vermiculite support has an absorption edge at the visible range, which is related to the natural light adsorption ability of Fe_2O_3 (E_g = 2.1 eV [23]). Compared with the ver sample, the absorption edge of the ver/HNO_3 sample presented a red-shift effect. The cause may be due to the leaching of some oxides with absorption edges at shorter wavelengths such as Al_2O_3 (E_g = 3.8 eV [24]) and MgO (E_g = 4.8 eV [25]). For the photocatalyst immobilized samples, the band gap was determined from the plots of $(\alpha h\vartheta)^2$ versus photon energy $h\vartheta$ using the Tauc equation [26]:

$$\alpha h\vartheta = E_d(h\vartheta - E_g)^{1/2}$$

where α is the optical absorption coefficient, $h\vartheta$ is the photon energy, E_g is the direct band gap, and E_d is a constant. The E_g value of TiO_2/ver is 3.1 eV, which agrees well with the reported value of anatase TiO_2 [27]. It can be seen that in the presence of Fe dopant, the TiO_2 band gap energy gradually decreases to 2.6 eV, which is consistent with the red shift of the absorption edge observed in the UV-vis spectra. This is normally assumed to be the overlapping conduction bands between Ti^{+4} of TiO_2 and the 3d electrons of Fe^{+3} ion, reducing the band gap energy of TiO_2 [28 - 30].

3.5. Adsorption and photocatalytic activities

In general, the contribution of both adsorption and photocatalysis with an immobilized photocatalyst was investigated in photocatalytic activity test. The degradation of ciprofloxacine under visible light irradiation using our photocatalyst samples was exhibited as depicted in Figure 7. The adsorption process was performed during 12 h in dark conditions to reach adsorption-desorption equilibrium. It was observed that the order of the adsorption capacity was ver/HNO_3 > Fe-TiO_2/ver > TiO_2/ver > ver, with adsorption efficiencies of 23 %, 20 %, 15 % and 6 %, respectively. Higher adsorption capability is proportional to larger surface area, which has been demonstrated in the literature. The visible light is turned on during 12 h after finishing the adsorption test to determine the photocatalytic oxidation efficiency. The results showed that the total ciprofloxacine degradation efficiencies of ver, ver/HNO_3, TiO_2/ver, Fe-TiO_2/ver were 10 %, 25 %, 38 % and 52 %, respectively. Both ver/HNO_3 and ver samples did not have

photocatalytic activity because the ciprofloxacine concentration decreased slightly after 12 hours of illumination (from 19 ppm to 18.7 ppm for ver and from 15.4 ppm to 15.2 ppm for ver/HNO_3). Meanwhile, the concentration of ciprofloxacine decreased immediately upon exposure to visible light (from 17 ppm to 12.5 ppm for TiO_2/ver and from 16 ppm to 9.8 ppm for Fe-TiO_2/ver), in which, the ciprofloxacine removal rate of the TiO_2/ver sample (23 %) was lower than that of the Fe-TiO_2/ver sample (33 %). This matched the red-shift results from the adsorption spectra, which enhanced the light absorption performance.

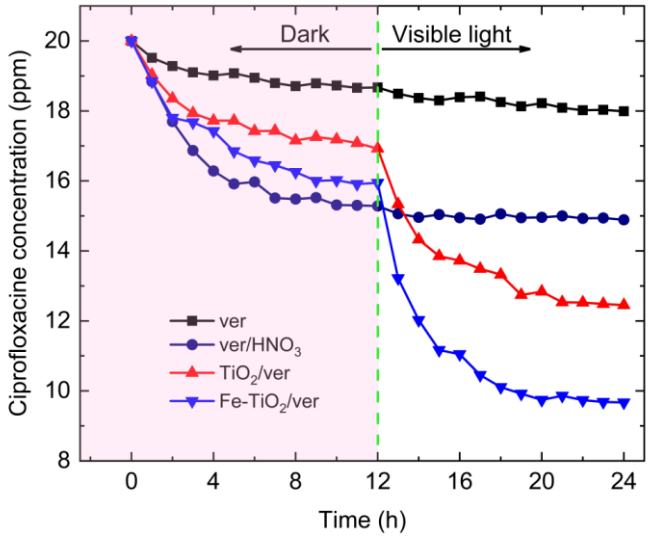

Figure 7. Adsorption and photocatalytic degradation profiles of ciprofloxacine aqueous solutions in a fixed bed reactor.

4. CONCLUSIONS

Fe-doped TiO_2 immobilized on vernimulite as a floating photocatalyst was successfully prepared by sol gel method. Before immobilizing the catalyst, vermiculite was treated with 40 % HNO_3 to improve its porous property, increasing the specific surface area 54 times from 6 m^2/g. Fe-doped TiO_2 nanoparticles with a size of 10 nm had a anatase phase. Fe dopant extended light absorption potential towards longer wavelengths. Therefore, the as-synthesized Fe-doped TiO_2 immobilized on vernimulite showed a better photodegradation rate of reactive ciprofloxacine under visible irradiation due to its small nanocrystal size. After 12 h of visible illumination, the ciprofloxacine degradation efficiency of Fe-doped TiO_2 immobilized vermiculite was 32 % while this value of pure TiO_2 immobilized vermiculite was only 23 %. These results also show the improvement of floating photocatalysts for the degradation of antibiotics in water environment using visible light sources.

Acknowledgements. This study is funded by the Vietnam Academy of Science and Technology (VAST) for senior researchers with code NVCC 30.02/22-23 and the Ministry of Science and Technology (MOST) of Viet Nam under national-level project: program 562, code /ĐTĐL.CN - 47.21.

CRediT authorship contribution statement. Nguyen Thi Hue: Investigation, project supervision, writing and reviewing, funding acquisition. Chu Viet Hai: Formal analysis, editing. Vu Van Tu: Methodology, formal analysis. Nguyen Xuan Dat: formal analysis. Luu Van Huyen: Investigation. Nguyen Manh Nghia: Investigation, writing the manuscript.

Declaration of competing interest. The authors declare that there is not any conflict of interest between them.

REFERENCES

1. Chen T., Liu Y., Lu J., Xing J., Li J., Liu T., and Xu Q. - Highly efficient detection of ciprofloxacin in water using a nitrogen-doped carbon electrode fabricated through plasma modification, New Journal of Chemistry **43** (2019) 15169-15176. https://doi.org/10.1039/C9NJ03511G.
2. Selvam A., Kwok K., Chen Y., Cheung A. , Leung K. S. Y., and Wong J. W. C. - Influence of livestock activities on residue antibiotic levels of rivers in Hong Kong, Environmental Science and Pollution Research **24** (2017) 9058-9066. https://doi: 10.1007/s11356-016-6338-5.
3. Verinda S. B., Muniroh M., Yulianto E., Maharani N., Gunawan G., and Amalia N. F. - Degradation of ciprofloxacin in aqueous solution using ozone microbubbles: spectroscopic, kinetics, and antibacterial analysis, Heliyon **8** (8) (2022) e10137. https://doi: 10.1016/j.heliyon.2022.e10137. eCollection 2022 Aug.
4. Costa L. N., Nobre F. X., Lobo A. O. and Matos J. M. E. - Photodegradation of ciprofloxacin using Z-scheme TiO_2/SnO_2 nanostructures as photocatalyst, Environmental Nanotechnology, Monitoring & Management **16** (2021) 100466. https://doi.org/10.1016/j.enmm.2021.100466.
5. Le N. D., Hoang A. Q., Hoang T. T. H., Nguyen T. A. H., Duong T. T., Pham T. M. H., *et al.* - Antibiotic and antiparasitic residues in surface water of urban rivers in the Red River Delta (Ha Noi, Viet Nam): concentrations, profiles, source estimation, and risk assessment, Environmental Science and Pollution Research **28** (2021) 10622-10632. https://doi:10.1007/s11356-020-11329-3.
6. Honarmandrad Z., Sun X., Wang Z., Naushad M., and Boczkaj G. - Activated persulfate and peroxymonosulfate based advanced oxidation processes (AOPs) for antibiotics degradation - A review, Water Resources and Industry **29** (2023) 100194. https://doi:10.1016/j.wri.2022.100194.
7. Cowie B. E., Porley V., and Robertson N. - Solar Disinfection (SODIS) Provides a Much Underexploited Opportunity for Researchers in Photocatalytic Water Treatment (PWT), ACS Catalysis **10** (20) (2020) 11779-11782. https://doi.org/10.1021/acscatal.0c03325.
8. Usman M. R., Prasasti A., Fajriyah S., Marita A. W., Islamiah S., Firdaus A. N., *et al.* - Degradation of ciprofloxacin by titanium dioxide (TiO_2) nanoparticles: Optimization of conditions, toxicity, and degradation pathway, Bulletin of Chemical Reaction Engineering & Catalysis **16** (4) (2021) 752-762. https://doi:10.9767/bcrec.16.4.11355.752-762.
9. Ali F., Moin-ud-Din G., Iqbal M., Nazir A., Altaf I., Alwadai N., *et al.* - Ag and Zn doped TiO_2 nano-catalyst synthesis via a facile green route and their catalytic activity for the remediation of dyes, Journal of Materials Research and Technology **23** (2023) 3626-637. https://doi.org/10.1016/j.jmrt.2023.02.011.
10. Nguyen L. T., Nguyen H. T., Pham T. D., Tran T. D., Chu H. T., Dang H. T., *et al.* - Visible Light Driven Photocatalytic Degradation of Ciprofloxacin by N, S Co-doped TiO_2: The Effect of Operational Parameters, Topics in Catalysis **63** (2020) 985-995. https://doi:10.1007/s11244-020-01319-7.

11. Li T., Abdelhaleem A., Chu W., Pu S., Qi F., and Zou J. - S-doped TiO_2 photocatalyst for visible LED mediated oxone activation: Kinetics and mechanism study for the photocatalytic degradation of pyrimethanil fungicide, Chemical Engineering Journal **411** (2021) 128450.
12. Tang C., Hu M., Fang M., Liu Y., Wu X., and Liu W. - Photocatalytic Property of TiO_2-Vermiculite Composite Nanofibers via Electrospinning, Nanoscale Research Letters **10** (2015) 276. http://doi:10.1186/s11671-015-0977-1.
13. Liu M., Zhang L., Xi B.D., Yu S., Hu X., and Hou L. A. - Degradation of ciprofloxacin by TiO_2/Fe_2O_3/zeolite catalyst-activated persulfate under visible LED light irradiation, RSC Advances **7** (2017) 51512-51520. https://doi.org/10.1039/C7RA08475G
14. Li D., Li R., Zeng F., Yan W., Deng M., and Cai S. - The photoexcited electron transfer and photocatalytic mechanism of g-C_3N_4/TiO_2 heterojunctions: Time-domain ab initio analysis, Applied Surface Science **614** (2023) 156104. https://doi.org/10.1016/j.apsusc.2022.156104.
15. Malakootian M., Nasiri A., and Amiri Gharaghani M. - Photocatalytic degradation of ciprofloxacin antibiotic by TiO_2 nanoparticles immobilized on a glass plate, Chemical Engineering Communications **207** (1) (2020) 56-72. http://doi:10.1080/00986445.2019.1573168.
16. Bui V. H., Vu T. K., To H. T., and Negishi N. - Application of TiO_2-ceramic/UVA photocatalyst for the photodegradation of sulfamethoxazole, Sustainable Chemistry and Pharmacy **26** (2022) 100617. http:// doi:10.1016/j.scp.2022.100617.
17. Wang L., Wang X., Cui S., Fan X., Zu B., and Wang C. - TiO_2 supported on silica nanolayers derived from vermiculite for efficient photocatalysis, Catalysis Today **216** (2013) 95-103. http://doi:10.1016/j.cattod.2013.06.026.
18. Machado L. C. R., Torchia C. B., and Lago R. M. - Floating photocatalysts based on TiO_2 supported on high surface area exfoliated vermiculite for water decontamination, Catalysis Communications **7** (8) (2006) 538-541. http://doi:10.1016/j.catcom.2005.10.020.
19. Nguyen N. M., Nguyen H. T., Negishi N., *et al.* - Effects of Ni doping and silica gel bead support on characteristics of TiO_2 catalyst, Journal of Electronic Materials **51** (2022) 6204-6212. https://doi.org/10.1007/s11664-022-09867-2.
20. Nghia N. M., Hue N. T., Thu M. T. A., *et al.* - Preparation and characterization of Fe-doped TiO_2 films covered on silicagel, Journal of Electronic Materials **45** (2016) 3795-3800. https://doi.org/10.1007/s11664-016-4524-3.
21. Jozefaciuk G. and Matyka-Sarzynska D. - Effect of acid treatment and alkali treatment on nanopore properties of selected minerals, Clays and Clay Minerals **54** (2006) 220-229. http://doi:10.1346/CCMN.2006.0540207.
22. Wei Z., Yingying L., Mengting M., *et al.* - A novel chitosan–vanadium-titanium-magnetite composite as a superior adsorbent for organic dyes in wastewater, Environment International **142** (2020) 105798. https://doi.org/10.1016/j.envint.2020.105798.
23. Parhizkar J. and Habibi M. H. - Synthesis, characterization and photocatalytic properties of Iron oxide nanoparticles synthesized by sol-gel autocombustion with ultrasonic irradiation, Nanochemistry Research **2** (2) (2017) 166-171. http://doi:10.22036/NCR.2017.02.002.

24. Alamouti A. F., Nadafan M., Dehghani Z., Ara M. H. M., and Noghreiyan A. V. - Structural and Optical Coefficients Investigation of γ-Al_2O_3 Nanoparticles using Kramers - Kronig Relations and Z - scan Technique, Journal of Asian Ceramic Societies **9** (1) (2021) 366-37. http://doi:10.1080/21870764.2020.1869881.
25. Almontasser A., Parveen A., and Azam A. - Synthesis, characterization and antibacterial activity of Magnesium Oxide (MgO) nanoparticles, IOP Conference Series: Materials Science and Engineering **577** (2019) 012051. http://doi: 10.1088/1757-99X/ 577/1/012051.
26. Thi P. T. V, Dinh T. T, Viet C. D. - Novel N,C,S-TiO_2/WO_3/rGO Z-scheme heterojunction with enhanced visible-light driven photocatalytic performance, Journal of Colloid and Interface Science **610** (2022) 49-60. https://doi.org/10.1016/j.jcis. 2021.12.050.
27. Verena P., Paul E., Shunyi L., *et al.* - Energy band alignment between anatase and rutile TiO_2, The Journal of Physical Chemistry Letters **4** (23) (2013) 4182-4187. https://doi.org/10.1021/jz402165b.
28. Abderrahim E. M., Imane A., Omar Z., *et al.* - Physico-chemical characterization and photocatalytic activity assessment under UV-A and visible-light irradiation of iron-doped TiO_2 nanoparticles, Arabian Journal of Chemistry **16** (12) (2023) 105331. https://doi.org/ 10.1016/j.arabjc.2023.105331.
29. Thi T. T. L, Dinh T. T., Thi H. D. - Remarkable enhancement of visible light driven photocatalytic performance of TiO_2 by simultaneously doping with C, N, and S, Chemical Physics **545** (2021) 111144. https://doi.org/10.1016/j.chemphys.2021.111144.
30. Thuy L. T. T, Lan N. T, Trinh T. D., Noi N. V. - Enhanced photocatalytic degradation of Rhodamine B using C/Fe co-doped Titanium dioxide coated on activated carbon, Journal of Chemistry **2019** (2019) 2949316. https://doi.org/10.1155/2019/2949316.